FME HighEFF

Centre for an Energy Efficient and Competitive Industry for the Future

Deliverable D2_3.2018.03

Effects from choice of thermodynamic and transport properties on heat exchanger design

Delivery date: 2018-12-20

Organisation name of lead beneficiary for this deliverable:

SINTEF Energy Research

HighEFF- Centre for an Energy Efficient and Competitive Industry for the Future is one of Norway's Centre for Environment-friendly Energy Research (FME). Project co-funded by the Research Council of Norway and Industry partners. Host institution is SINTEF Energi AS.		
Dissemination Level		
PU	Public	x
RE	Restricted to a group specified by the consortium	

Deliverable number:	D2_3_2018.04
ISBN number:	
Deliverable title:	Effects from choice of thermodynamic and transport properties on heat exchanger design
Work package:	RA 2.3
Deliverable type:	Memo
Lead participant:	SINTEF Energy Research

Quality Assurance, status of deliverable		
Action	Performed by	Date
Verified (WP leader)	Geir Skaugen	2018-12-19
Reviewed (RA leader)	Armin Hafner	2018-12-19
Approved (dependent on nature of deliverable)*)		

*) *The quality assurance and approval of HighEFF deliverables and publications have to follow the established procedure. The procedure can be found in the HighEFF eRoom in the folder "Administrative > Procedures".*

Authors		
Author(s) Name	Organisation	E-mail address
Goran Durakovic	SINTEF Energy Reseach	Goran.Durakovic@sintef.no
Hans Langva Skarsvåg	SINTEF Energy Research	Hans.Skarsvag@sintef.no
Geir Skaugen	SINTEF Energy Research	Geir.Skaugen@sintef.no

Abstract

Table of Contents

1 Introduction

Today, computational models are often used in the design of thermodynamic processes and during operation to test various operating scenarios. This approach is chosen because it is both cheaper and faster than experimental testing. Such simulators are often built upon several underlying models that each describe different parts of the process, where for instance one model calculates the behaviour of the working fluid everywhere in the process, and each component in the process has some model that calculates how that component performs.

In this work, we looked into models for the working fluid. In particular, we have chosen to investigate what influence models for transport properties, i.e. thermal conductivity and dynamic viscosity, have on the design of the heat exchangers in a low-temperature organic Rankine cycle. A secondary objective is also to investigate how such models influence the overall process as well. This work is a continuation of a previous deliverable, where we investigated the role of equations of state on the optimal process parameters in a similar cycle. To expand on that research, we shifted the focus from equations of state to models for the more elementary transport properties.

The thermal conductivity of a fluid is involved in any heat exchange that the fluid experiences, where a high thermal conductivity allows for large heat transfers in a given time. If the model used for calculating thermal conductivity of our fluid consistently underestimates its true value, then the calculated heat exchanger may be too large and transfer more heat than intended. This is unacceptable in scenarios where the temperature of the heat exchanging fluids must be strictly controlled. Even if the temperatures of the fluids do not need to be within tight tolerances, larger heat exchangers will lead to a higher investment cost and will use more space and weight than necessary. We include the thermal conductivity in our study to ascertain its influence on the heat exchanger size.

The dynamic viscosity is involved wherever a fluid flows and is correlated most often with pressure drop. When comparing two fluids under the same conditions, the more viscous fluid will experience a higher pressure drop compared to the less viscous one. Pressure drop will negatively influence the performance of a Rankine cycle, as it will lead to a decreased pressure ratio across the expander. As different models for viscosity will each calculate a unique value of the viscosity at a given state, we expect that the reported performance will vary as one changes the viscosity model under a set of design process parameters. However, it is not clear how the system will change when the optimizer can change the process parameters to better suit the viscosity model in question. We therefore set out to investigate the role of the viscosity model as well in this investigation.

2 Model

The overarching model is built using SINTEF's FlexCS framework. The general qualities and methods of FlexCS have been described previously in Deliverables [1] and [2]. Linked to FlexCS is Thermopack and Thermphys that provide the model with fluid property data. These models are described in [3]. In this investigation, we used propane as the working fluid with PR-Peneloux as the equation of state. PR-Peneloux was chosen because it is fast, which allows us to generate a large dataset quickly. This equation of state is known to not be as accurate as other more computationally demanding models, but any changes in optimal process parameters because of the chosen thermal conductivity model or viscosity model should still be apparent.

In real operation, the flow will experience pressure drop when it flows in the heat exchangers and the pipes connecting the components together. This simplified model ignores the pressure drop in the pipes, so that the only pressure loss in the cycle is found in the heat exchangers.

In this investigation, we have used a generic geometry heat exchanger model, meaning that the geometries of the heat exchangers are described by a length, and a number of hot and cold tubes. Between the hot and cold tubes there is a perfect heat exchange, so no heat is lost to the surroundings. Figure 1 illustrates the simplified heat exchanger geometry. The heat exchangers are subdivided into 50 elements of equal enthalpy difference. The evaporator model begins at the outlet, meaning in the hot end, whereas the opposite is true for the condenser.

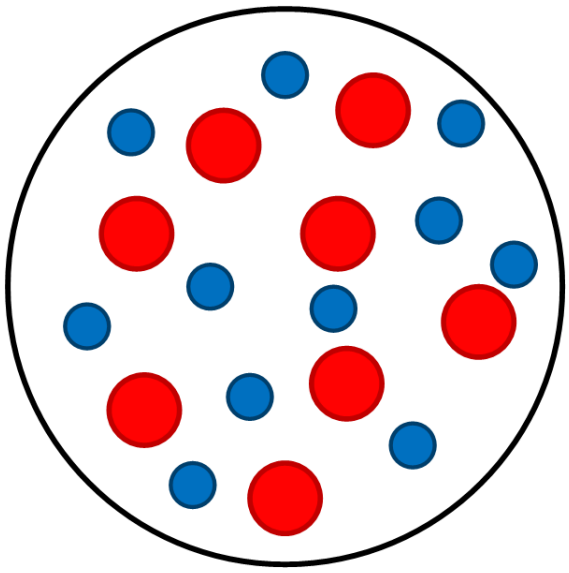

Figure 1: Visual description of generic heat exchanger geometry. (Hot tubes in red, warm tubes in blue.)

The implementation of models for thermal conductivity and dynamic viscosity have been described in [4] (attached). This investigation looks into using the model by Chung and the TRAPP and TRAPP-McLinden methods for the thermal conductivity model. Of these we believe that the TRAPP-McLinden is the most

accurate, as the TRAPP method is the most accurate far away from the critical point, while McLinden is the most accurate close to it. Our implementation of these two models includes smoothing between these two models as the fluid's state transitions from away from the critical point to close to the critical point.

The chosen viscosity models are the TRAPP and its modified version, TRAPPV. Our selection is limited as these are the only two models that currently work within the FlexCS framework. Regardless, having two different viscosity models should illuminate the influence of viscosity on the cycle.

3 Model parameters and method

The process optimizer works by finding the set of parameters that maximize or minimize and objective function, and takes into account a list of constraints that are set. The objective function in this work is the net power developed by the process. One of the constraints in the model is that the optimizer can only allocate a certain total size to the heat exchangers, but it is free to distribute this total to the heat exchangers in the model in order to maximize the net power production of the cycle. In this work, we investigated different values for the total size, in order to investigate different scenarios for the thermal conductivity and dynamic viscosity models.

The parameters that describe the case used in the investigation is summarized in Table 1. These were held constant as the different models have been investigated. The other parameters, shown in

Table 2, were free to be changed by the optimizer. Additionally, the total heat exchanger area was manually varied between 100 and 200 m^2 in step of 50, to investigate whether any differences arose when the optimizer utilized more area.

Table 1: Specifications for the cycle.

Heat source			
	Fluid	[-]	Air equivalent
	Inlet temperature	[°C]	150
	Mass flow	[kg/s]	5
	Minimum temperature	[°C]	80
Heat sink			
	Fluid	[-]	Water
	Inlet temperature	[°C]	10
Working fluid			
	Fluid	[-]	Propane
Cycle parameters			
	Evaporator hot side heat transfer coefficient	[W/(m^{2}K)]	100
	Evaporator cold side tube diameter	[mm]	1
	Condenser cold side number of tubes	[-]	1500
	Condenser hot side tube diameter	[mm]	1
	Condenser cold side tube diameter	[mm]	3
	Expander isentropic efficiency	[%]	85
	Pump isentropic efficiency	[%]	70
	Generator efficiency	[%]	95
	Motor efficiency	[%]	95
	Maximum heat exchanger area	[m^2]	100/150/200

The initial values for each parameter in Table 2, and the maximum and minimum limits of each parameter, must be set prior to starting an optimization. These values are not included in the table as they were adjusted between the different total heat exchanger area cases.

Table 2: Variable parameters for the optimizer.

Parameter	Unit
Heat sink mass flow rate	[kg/s]
Expander inlet pressure	[bar]
Expander inlet temperature	[°C]
Working fluid mass flow rate	[kg/s]
Pump inlet temperature	[°C]
Evaporator length	[m]
Evaporator cold side number of tubes	[-]
Condenser length	[m]
Condenser hot side number of tubes	[-]

4 Results

Figure 2: Calculated net power versus total heat exchanger area.Figure 2 shows the calculated net power for all the investigated heat exchanger areas with the different combinations of models for thermal conductivity and dynamic viscosity. We see that there are no major differences for the first two heat exchanger areas (100 and 150), but the results diverge significantly for the final datapoint (heat exchanger area equal to 200.) The results for this data point do not seem to be valid, as will be discussed later in this memo.

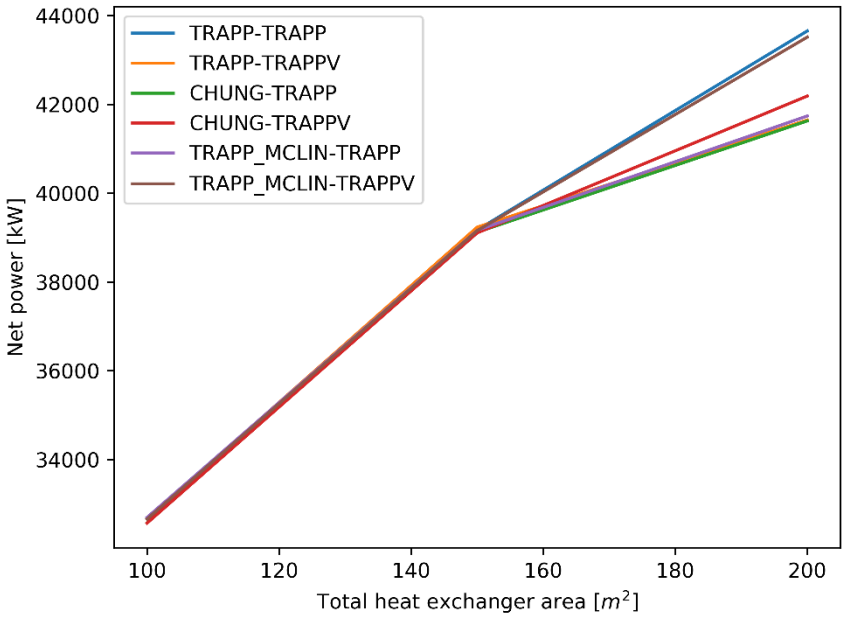

Figure 2: Calculated net power versus total heat exchanger area.

Table 3 shows the optimized geometries for each solution in Figure 2. For the first two heat exchanger area cases, we see that there are some differences in how the simple heat exchangers are shaped, but the heat transfer areas remain very similar. For example, in Table 3 when the total heat exchanger area is 100 m^2, we see that there are essentially two sets of data for the evaporator: either the length is around 10 m and there are around 2500 tubes, or the length is closer to 9 m and the number of tubes increases to above 2800. Regardless, the area for the evaporator in all of these cases remains very close to 84 m^2. The changes in heat exchanger designs shown in Table 3 are not reflected in any notable performance difference in Figure 2, suggesting that in this cycle simulator, the shape of the heat exchangers are much less important than the calculated total heat exchanger area. It seems that these differences come about as a result of numerical noise where either solution can be accepted by the optimizer, as they both lead to roughly the same net power. Investigating Table 3, but for total heat exchanger area of 150 m^2, we see that the model combinations that gave a small length but high tube count in the previous total heat exchanger area case do not necessarily give relatively small lengths and high tube counts for this case. Because it seems somewhat random which model combinations give a small heat exchanger length and high tube count, it seems more likely that it is indeed caused by numerical noise.

Table 4 shows the operating characteristics of the heat exchangers. When inspecting the table, keep in mind that the pump inlet temperature is directly related to the condensation pressure. In Table 4 we see a large variation in the evaporator pressure loss for the first two heat exchanger area cases compared to the other parameters. Comparing Table 4 and Table 3, we see how the pressure loss in the heat exchanger is correlated with its geometry: a long heat exchanger with few tubes will have a significantly higher pressure drop compared to a short tube with many tubes. This is true regardless of the chosen models for thermal conductivity and dynamic viscosity.

Table 3: Optimized simple heat exchanger geometries.

	Thermal conductivity model	Dynamic viscosity model	Evaporator length	Evaporator number of tubes	Evaporator area	Condenser length	Condenser number of tubes	Condenser area
Total HX area = 100m^2	TRAPP	TRAPP	9.07	2811	84.08	1.42	3400	15.92
	TRAPP	TRAPPV	8.86	2881	84.15	1.42	3387	15.85
	CHUNG	TRAPP	10.19	2490	83.68	1.43	3468	16.32
	CHUNG	TRAPPV	9.99	2546	83.90	1.43	3403	16.10
	TRAPP_MCLIN	TRAPP	8.55	2979	84.00	1.42	3414	16.00
	TRAPP_MCLIN	TRAPPV	10.21	2496	84.06	1.43	3374	15.94
Total HX area = 150m^2	TRAPP	TRAPP	10.68	3511	123.68	1.90	4209	26.32
	TRAPP	TRAPPV	10.85	3500	125.24	1.80	4178	24.76
	CHUNG	TRAPP	11.28	3306	123.01	1.92	4262	27.00
	CHUNG	TRAPPV	11.06	3372	123.00	1.95	4200	27.00
	TRAPP_MCLIN	TRAPP	11.36	3280	122.88	1.93	4269	27.11
	TRAPP_MCLIN	TRAPPV	11.01	3384	122.88	1.96	4199	27.12
Total HX area = 200m^2	TRAPP	TRAPP	12.52	3518	145.30	3.35	4906	54.14
	TRAPP	TRAPPV	11.40	4238	159.39	2.74	4500	40.61
	CHUNG	TRAPP	12.62	3863	160.88	2.82	4204	39.12
	CHUNG	TRAPPV	11.73	4034	156.03	2.96	4509	43.97
	TRAPP_MCLIN	TRAPP	10.32	4794	163.14	2.25	4969	36.86
	TRAPP_MCLIN	TRAPPV	11.82	4155	162.01	2.64	4370	37.99

Table 4: Heat exchanger operating characteristics for the optimized solutions.

	Thermal conductivity model	Dynamic viscosity model	Evaporator pressure loss	Condenser pressure loss	Pump inlet temperature	Expander inlet pressure
Total HX area = 100m^2	TRAPP	TRAPP	0.62	0.80	21.6	43.2
	TRAPP	TRAPPV	0.58	0.79	21.6	43.6
	CHUNG	TRAPP	0.85	0.77	21.7	43.8
	CHUNG	TRAPPV	0.80	0.79	21.5	44.1
	TRAPP_MCLIN	TRAPP	0.53	0.80	21.5	43.2
	TRAPP_MCLIN	TRAPPV	0.87	0.82	21.5	43.3
Total HX area = 150m^2	TRAPP	TRAPP	0.52	0.82	20.0	57.1
	TRAPP	TRAPPV	0.54	0.78	20.5	57.2
	CHUNG	TRAPP	0.62	0.80	20.2	56.7
	CHUNG	TRAPPV	0.58	0.84	19.9	56.8
	TRAPP_MCLIN	TRAPP	0.63	0.80	20.2	56.8
	TRAPP_MCLIN	TRAPPV	0.57	0.84	19.7	57.0
Total HX area = 200m^2	TRAPP	TRAPP	0.57	0.90	18.3	62.5
	TRAPP	TRAPPV	0.37	0.87	18.4	64.5
	CHUNG	TRAPP	0.47	0.85	18.5	55.2
	CHUNG	TRAPPV	0.42	0.98	18.1	66.4
	TRAPP_MCLIN	TRAPP	0.28	0.60	20.7	66.7
	TRAPP_MCLIN	TRAPPV	0.39	0.77	19.3	57.7

5 Discussion

It is remarkable that the results are so similar for all the models when the total heat exchanger area is less than 200 m^2. Let us first investigate the data for the case when the total heat exchanger area is equal to 200 m^2, in order to discover what sets it apart.

5.1 Diverging results for when the total heat exchanger area is equal to 200 m^2.

For a given value of total heat exchanger area, the only differences between the various results are the chosen models for the thermal conductivity and dynamic viscosity. For each heat exchanger, at the start of each of the 50 elements, we reported the values of the thermal conductivity and dynamic viscosity, as well as the calculated heat transfer coefficient and elementwise pressure drop. These allow us to explore how the aforementioned characteristics vary at the different states inside the heat exchangers. These are plotted in Figures Figure 3Figure 3 and Figure 4 for when the total heat exchanger area is equal to 200 m^2.

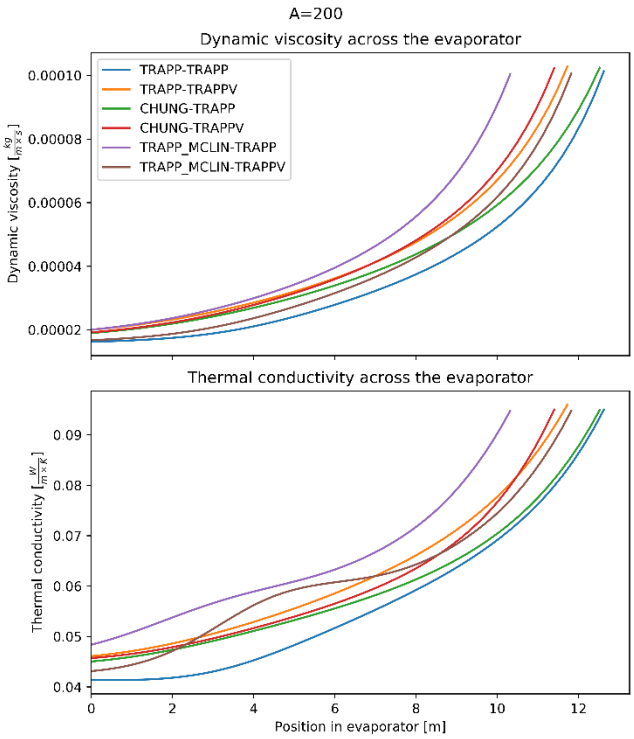

Figure 3: Variation of dynamic viscosity and thermal conductivity in the evaporator for total heat exchanger area = 200.

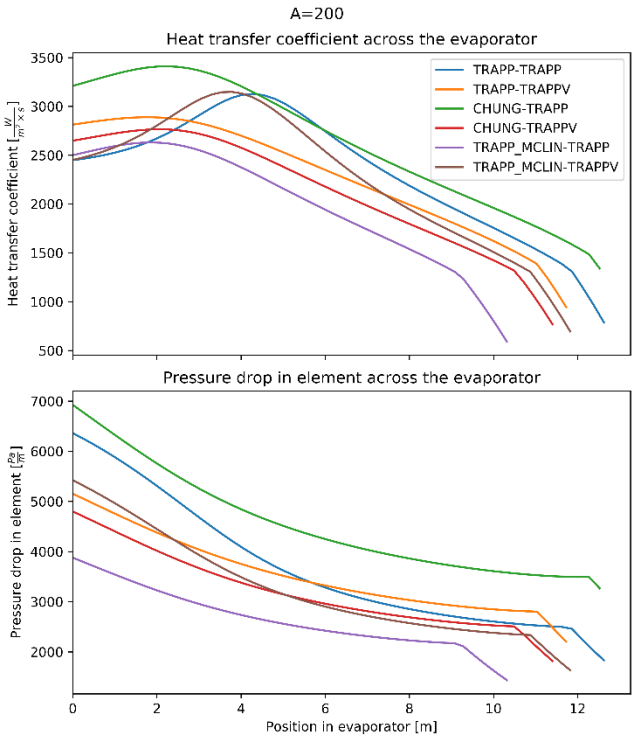

Figure 4: Variation of heat transfer coefficient and elementwise pressure drop in the evaporator for total heat exchanger area = 200.

Figure 3 does not show any results that are obviously suspicious. However, the same is not true for the reported heat transfer coefficients and elementwise pressure drops. Toward the end of the heat exchanger, both of these characteristics experience a sharp and sudden decline. Since the working fluid was

supercritical everywhere in the evaporator, we expected that the curves would be smoother. Compare Figure 4 with Figure 5, where the same characteristics have been plotted, but this time for a total heat exchanger area of 100 m^2 instead of 200 m^2.

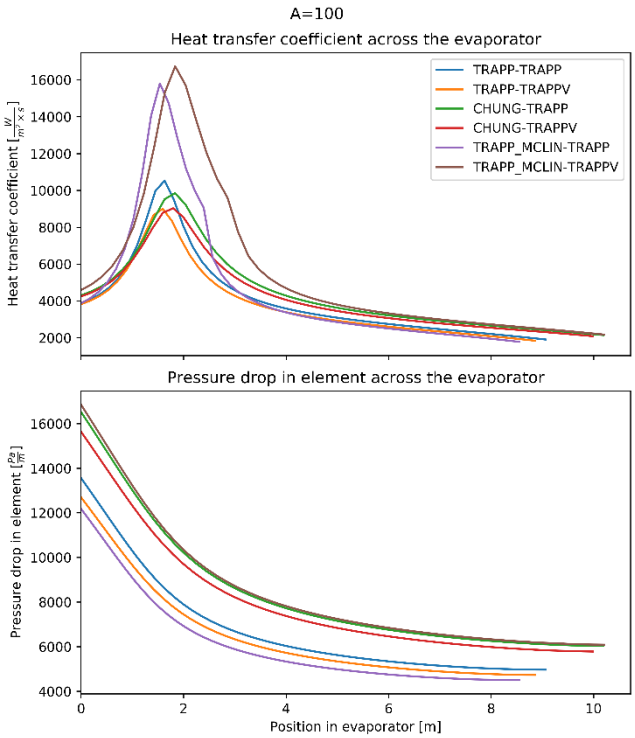

Figure 5: Variation of heat transfer coefficient and elementwise pressure drop in the evaporator for total heat exchanger area = 100.

Figure 5 shows what we expect from the variation in these two parameters. The development of the pressure drop is smooth without any suspicious sudden changes in the curve. The curve for the heat transfer coefficient spikes at roughly the same position for all the models. This occurs because the working fluid comes close to its critical point, leading to a higher thermal conductivity, as explained in detail in [4]. Due to the suspicious nature of Figures Figure 3Figure 3 and Figure 4, we have chosen to neglect it from further discussion.

5.2 Analysing data for A_{tot} = 100 and 150 m^2

In Appendix A, the detailed evaporator plots are available for all areas. From Figures Figure 17 and Figure 19 we see that when the model for thermal conductivity is TRAPP-McLinden, the thermal conductivity is consistently higher. This is reflected in the calculated heat transfer coefficients, where the peak heat transfer coefficient for TRAPP-McLinden for the A_{tot} = 100 m^2 case is almost twice as high as for the other models. Based solely on this observation, one would expect that the optimizer would calculate a higher net power when TRAPP-McLinden is the chosen model for thermal conductivity. However, from the same figures, we see that the pressure drop is also the highest when TRAPP-McLinden is the model for thermal conductivity. The increased heat transfer coefficient will improve the performance for a given value of A_{tot},

but the pressure loss will reduce it. It seems that these balance each other fairly closely, resulting in similar reported net power values.

It may be that the results in this work as so similar due to the methodology used. We have specified a maximum heat exchanger area that the optimizer can use, and used the optimizer to have it find the set of process parameters that maximize net power. With this approach, the optimizer will use all of the available area in all cases, unless the minimum temperature pinch is reached. This can only happen for very large values of maximum heat exchanger area and did not occur in this investigation. However, because the optimizer will always use all the available heat exchanger area, the differences in component sizes will be lost. Another approach could have been to specify a net power from the cycle, or a heat exchanger duty, and have the optimizer minimize the required area. This was not possible with this FlexCS model and was therefore not performed. However, with this approach, perhaps we would see greater distinction between the models.

5.3 Unrestricted heat source

In the initial optimizations, we investigated cases where the heat source could not be cooled to below 80°C. To investigate whether the similar results would continue in other cases, we also investigated the same case, but without a lower limit on the heat source temperature. We also expanded the lower limit of areas to investigate more challenging cases for the optimizer, hoping that this would lead to divergent but valid solutions.

Figure 6 shows how the net power changes with total heat exchanger area for each combination of thermal conductivity model and dynamic viscosity model. Even here there are no apparent differences in the objective function.

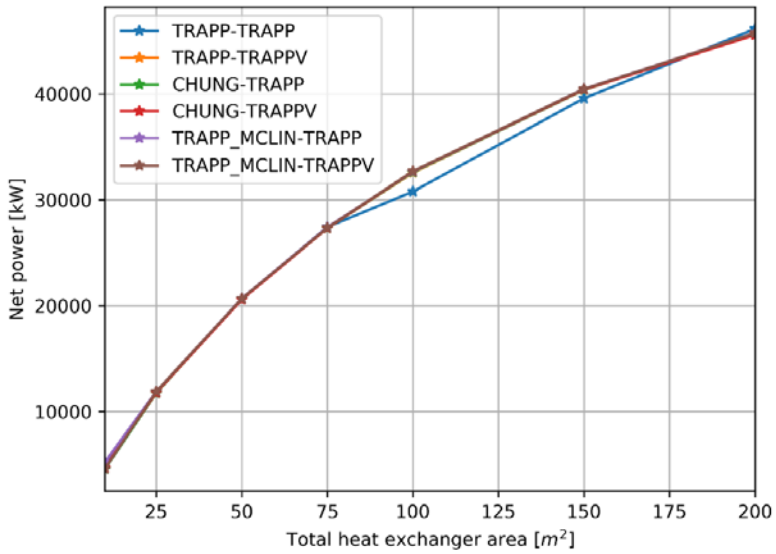

Figure 6: Net power versus total heat exchanger area for unrestricted heat source.

Similar to the previous results, we find a larger difference in the thermal conductivities and dynamic viscosities, and consequently also in the calculated elementwise pressure drops and heat transfer coefficients. Inspect, for example, Figures Figure 7 to Figure 10. It seems that while the choice of model does influence the estimated thermal conductivity and dynamic viscosity, and thus subsequently also the heat transfer coefficient and pressure drop, it does not translate into any discernible difference in the reported net power.

When inspecting Figure 7, one should not be alarmed by interval where the thermal conductivity and dynamic viscosity are constant, and then suddenly jump. This occurs because the working fluid is in the two-phase region where it is constant, and when it jumps to the right in the graph, the working fluid is completely liquid. In the fluid model, when the working fluid is in a single phase then liquid and vapour properties are identical, and this is what we see in Figure 7.

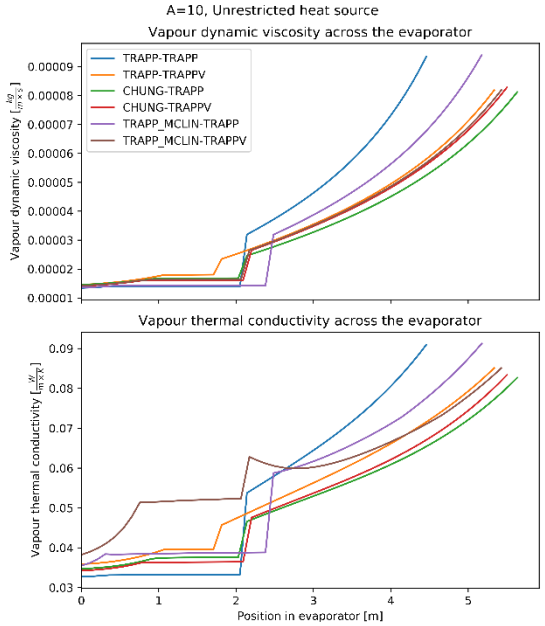

Figure 7: Variation of dynamic viscosity and thermal conductivity in the evaporator for total heat exchanger area = 10 and unrestricted heat source.

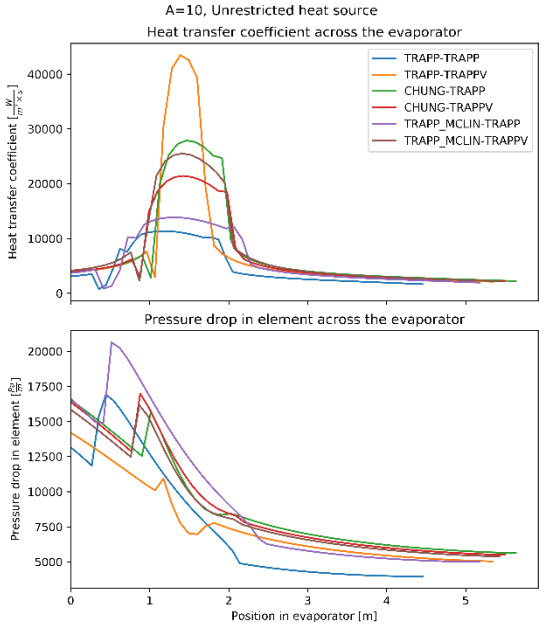

Figure 8: Variation of heat transfer coefficient and elementwise pressure drop in the evaporator for total heat exchanger area = 10 and unrestricted heat source.

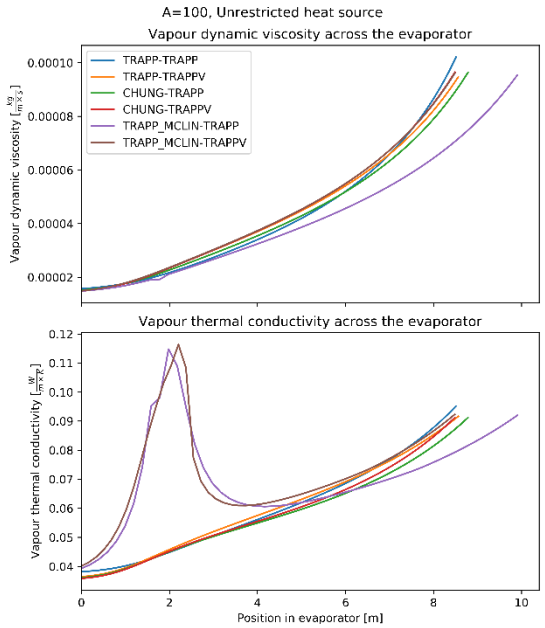

Figure 9: Variation of dynamic viscosity and thermal conductivity in the evaporator for total heat exchanger area = 100 and unrestricted heat source.

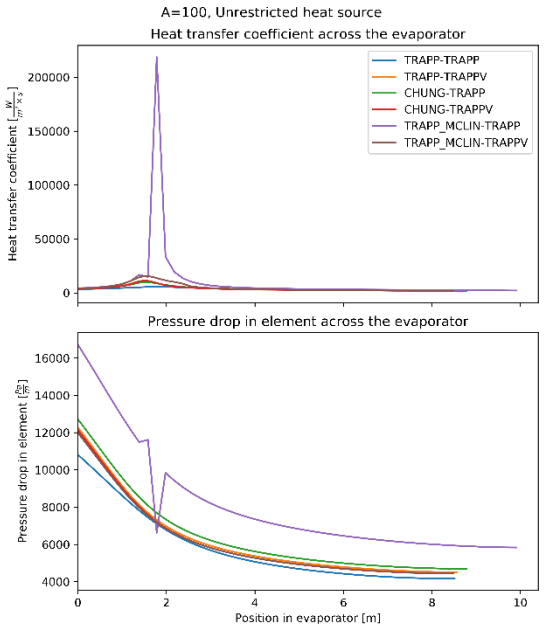

Figure 10: Variation of heat transfer coefficient and elementwise pressure drop in the evaporator for total heat exchanger area = 100 and unrestricted heat source.[1]

5.4 Increasing the heat transfer coefficient on the heat source side

One possibility for the very similar results is that the majority of the thermal resistance in the evaporator is on the heat source side. The heat transfer coefficient for the heat source is constant in this model, unlike for all the other flows. Investigating for example Figure 8, we see that the heat transfer coefficient of the working fluid in the evaporator is much higher than 100 $\frac{W}{m^2 \times K}$. It may be that the heat transfer coefficient of the heat source is so restrictive that the differences between the thermal conductivity and dynamic viscosity models are somehow lost. To test this possibility, we investigated the results when the heat transfer coefficient of the heat source is set to 20,000 $\frac{W}{m^2 \times K}$ instead of 100. Heat transfer coefficients this high may be reached for example under phase change, and it is thus interesting to see if the choice of models matter more in cases where the heat transfer coefficient of the heat source is very high.

Figure 11 shows how the net power develops for the different heat exchanger areas when the heat transfer coefficient is increased for the heat source. In Figure 11 we can see that, as before, there are few differences in the calculated net power between the chosen models. The combination of TRAPP-TRAPP seems to output a significantly different result for when the total heat exchanger area is equal to 75 m^2, but this data point seems more like an outlier when evaluating this model combination for the other data points as well.

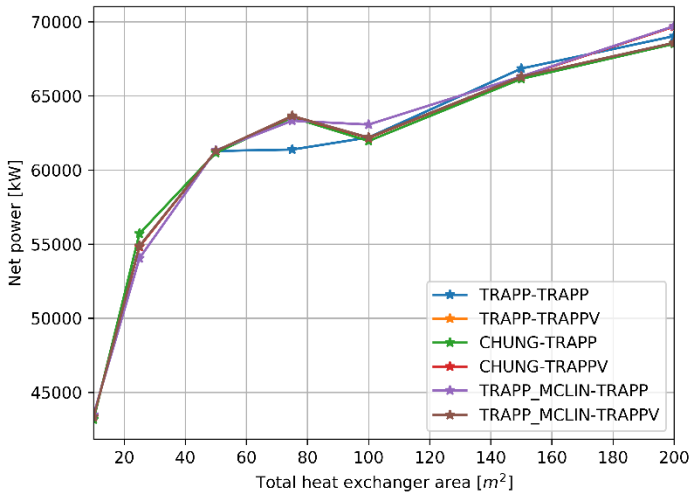

Figure 11: Net power versus total heat exchanger area for a heat source with high heat transfer coefficient.

[1] The large spike in heat transfer coefficient is caused by the working fluid coming very close to its critical point. This results in an extremely large estimation for the specific heat capacity, which eventually results in a large heat transfer coefficient.

While the reported net power may be similar between the six combinations of thermal conductivity and dynamic viscosity models, the allocation of available heat exchanger area, and thus process design, may vary. Figure 12 shows how much of the total area is dedicated to the condenser in each case (where the remaining available area is used by the evaporator.) We see that here too the results are nearly identical. It is therefore safe to say that having a higher heat transfer coefficient on the heat source side does not provoke a difference between the thermal conductivity and dynamic viscosity model combinations.

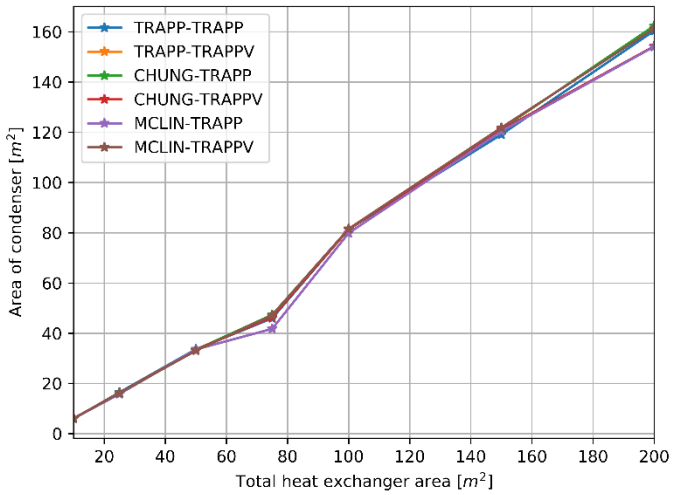

Figure 12: Allocation of area to condenser when the heat transfer coefficient of the heat source is set to 20000.

5.5 Manually adjusting the thermal conductivities and dynamic viscosities

One final explanation to why the results are so similar is that the different models all calculate very similar values for thermal conductivity and dynamic viscosity. Reviewing Appendix A, we see that they indeed are very similar, and only the thermal conductivity seems to diverge in a limited range in the evaporator. It is no coincidence that they diverge only in this limited range: this occurs because the working fluid is close to the critical point in this range, and as detailed by [4], only the TRAPP-McLinden model for thermal conductivity takes into account the increase in thermal conductivity close to the critical point. Nonetheless, because the calculated thermal conductivities and dynamic viscosities are so similar when the state of the working fluid is not close to the critical point, then it is reasonable that their optimized solutions are also very similar. To investigate what happens when the values for the thermal conductivities are very different, we investigated how the optimized system differed when the values for thermal conductivity and dynamic viscosity were multiplied by a factor to increase or decrease their calculated values. These factors were 0.1 and 2, so the calculated values were lowered by 90% or increased by 100%. The model used to calculate the thermal conductivity before the factor was applied was the TRAPP-McLinden model, and the equivalent model for the dynamic viscosity was the TRAPPV model.

Figure 13 shows the optimized net power when the calculated thermal conductivity and dynamic viscosity are multiplied with these factors, with the four different combinations. The unchanged case, where the factor is 1 (i.e. no change) is also included in the figure.

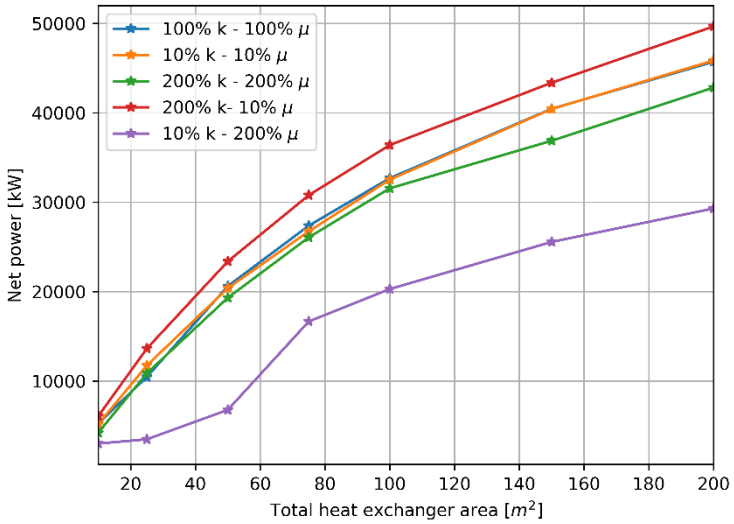

Figure 13: Net power versus total heat exchanger area with thermal conductivity and dynamic viscosity increased and decreased by factor.

Figure 13 reveals some interesting results. We see that when the thermal conductivity and dynamic viscosity are both increased or lowered simultaneously, their reported net power are very similar. The results only start diverging across the range of total heat exchanger areas when the thermal conductivity is increased while the dynamic viscosity is decreased or vice versa. How the results changed is not as surprising, where the net power decreased significantly when the thermal conductivity was low and the dynamic viscosity was high, and conversely, it increased when the thermal conductivity was high and the viscosity low. This falls in line with our expectations, as explained in Section 1.

Figure 14 shows how much of the area is distributed to the condenser when the thermal conductivity and dynamic viscosity is manually changed as here. Three out of the five curves develop fairly smoothly, while the final two do not experience the same steady increase. In particular, the case where the thermal conductivity is reduced and the dynamic viscosity is increased seems to allocate area to the condenser with no clearly discernible pattern. When the optimizer gives results like these, it is generally an indication that the optimization case is challenging for the model, and that it may therefore have found solutions that are not global optima. However, a general trend is that when the viscosity is increased, more area is dedicated to the condenser. This is likely because the viscosity of the working fluid in the condenser is larger than in the evaporator, and when the thermal conductivity is doubled everywhere in the system, it is increased more for the fluid in the condenser in absolute terms. All other things equal, this would have led to a larger increase in pressure loss in the condenser than in the evaporator, and increasing the condenser heat exchanger area may be a way to counteract this larger pressure loss. This is shown in Figure 15. For the case where thermal conductivity is decreased and dynamic viscosity is increased (purple line), notice how the condenser pressure loss is the smallest when the condenser area is most dissimilar to the other curves.

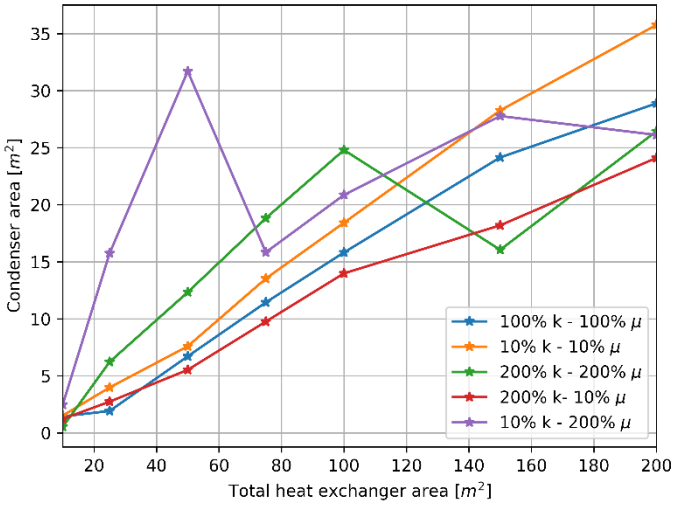

Figure 14: Area distributed to condenser when the thermal conductivity and dynamic viscosity are manually increased and decreased by factor.

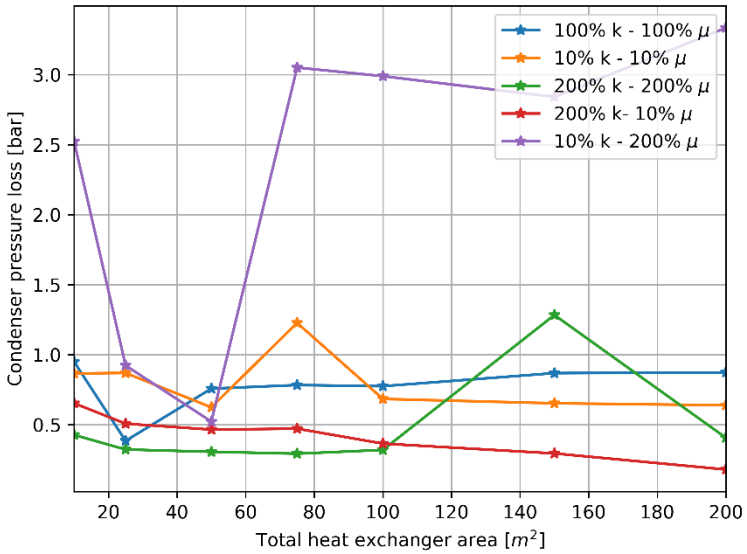

Figure 15: Pressure loss in condenser for each heat exchanger area when thermal conductivity and dynamic viscosity are manually increased and decreased by factor.

Also, for the case when the thermal conductivity is increased and the dynamic viscosity is decreased (red line), notice how the condenser area is always lower than for the purple line (10% k – 200% μ). This case also had the among the smallest pressure losses in the condenser, as seen in Figure 15. It thus seems that the primary effect of the thermal conductivity and dynamic viscosity is on the dimensioning of the condenser in the system: an increase in thermal conductivity or a decrease in dynamic viscosity will lead to

a smaller pressure loss and less heat exchanger area to the condenser, thereby leaving more area to be used by the evaporator.

6 Conclusion

In this work, we investigated how optimal cycle designs from FlexCS would change when using three different models for thermal conductivity and two different models for dynamic viscosity. No significant differences seemed to come from changing these models, either in calculated net power or design of heat exchangers. Changing the heat source parameters, by removing the lower temperature limit or increasing the heat transfer coefficient, did not lead to more divergent results.

When manually increasing by 100 % or decreasing by 90% the calculated thermal conductivities and dynamic viscosities, we were able to get results that clearly distinguished themselves from one another. Interestingly, when the thermal conductivity and the dynamic viscosity were both increased or decreased simultaneously, the results did not change much from when they were unaltered. However, when one was decreased while the other increased, that is when the results clearly set themselves apart. It thus seems that when these two parameters are changed equally, then they also balance each other so that the net change is small.

We saw that all the combinations of models for thermal conductivity and dynamic viscosity gave very similar results, and only when these were manually lowered and increased, did we see a discernible difference in the calculated net power. When the net power was similar between the models, the distribution of total heat exchanger area was also similar, but there were some differences in the optimal heat exchanger geometries, but it seems that these differences arise from numerical noise rather than truly having different optimal designs.

Ultimately, it appears that for this generic heat exchanger model, the choice of models for the thermal conductivity and dynamic viscosity do not influence the results much, primarily because the calculated values of these two parameters from the different models are so similar. It may be that the choice of these models matters more when using heat exchanger models that simulate real heat exchanger designs in greater detail, and it would be interesting to investigate how the design of such heat exchangers would change when choosing between the different thermal conductivity and dynamic viscosity models. This investigation could be performed in a future work.

[1] B. Hagen, “Deliverable D3.1_2017_04 Numerical framework for power cycle simulation and optimization.” 2017.

[2] B. R. Knudsen, “Memo Numerical optimization methods in FlexHX / CS,” pp. 1–10, 2017.

[3] G. Skaugen, “Maintaining and adapting specially designed in-house tools for HXs,” 2012.

[4] H. Langva Skarsvåg, “Memo Hydrocarbon viscosity and thermal conductivity at high pressures,” pp. 1–14, 2018.

A All plots of dynamic viscosity, thermal conductivity, heat transfer coefficient and pressure drop in the evaporators

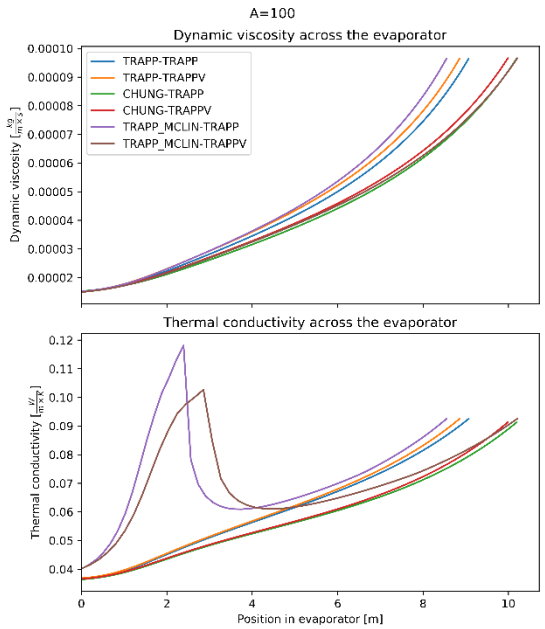

Figure 16: Variation of dynamic viscosity and thermal conductivity in evaporator for total heat exchanger area = 100.

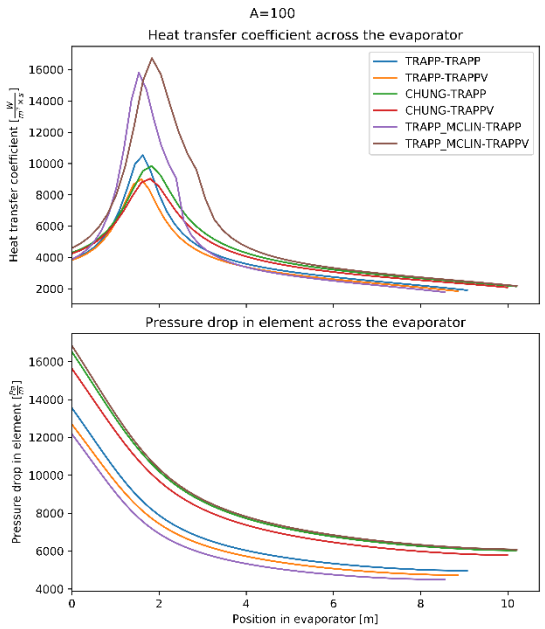

Figure 17: Variation of heat transfer coefficient and elementwise pressure drop in the evaporator for total heat exchanger area = 100.

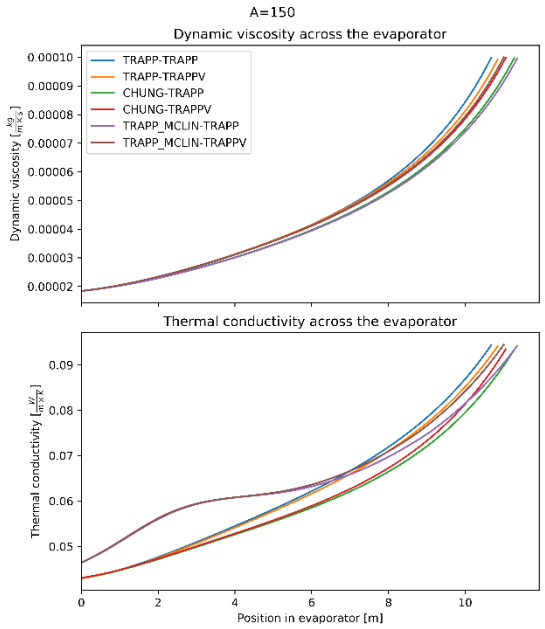

Figure 18: Variation of dynamic viscosity and thermal conductivity in evaporator for total heat exchanger area = 150.

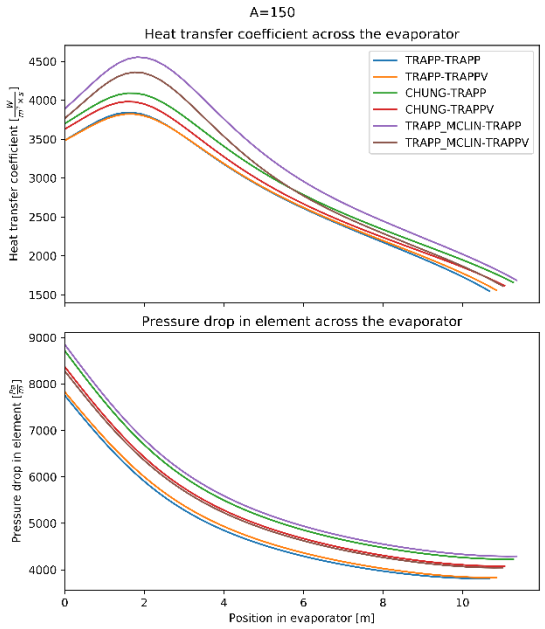

Figure 19: Variation of heat transfer coefficient and elementwise pressure drop in the evaporator for total heat exchanger area = 150.

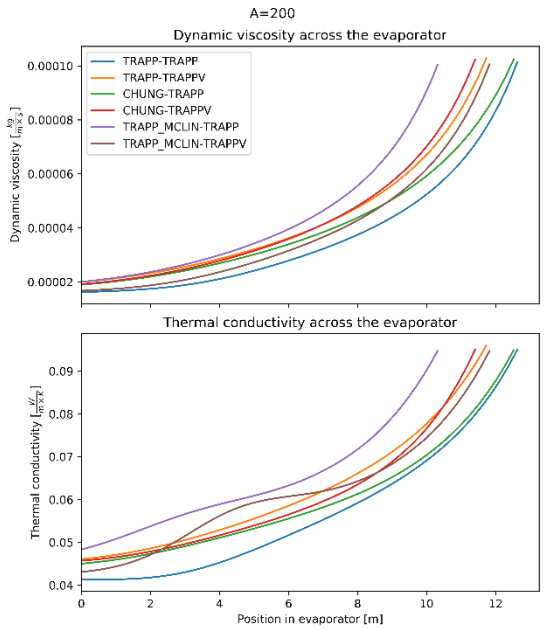

Figure 20: Variation of dynamic viscosity and thermal conductivity in evaporator for total heat exchanger area = 200.

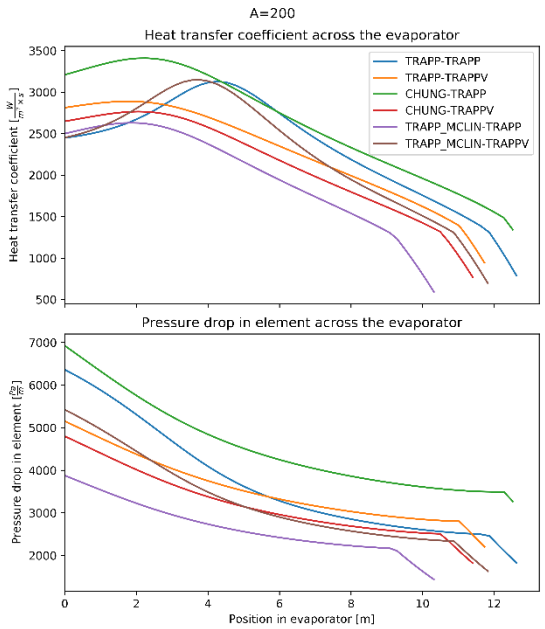

Figure 21: Variation of heat transfer coefficient and elementwise pressure drop in the evaporator for total heat exchanger area = 200.

B Description of transport models presented and evaluated in this work.

SINTEF

Contents

1 Introduction

This memo is based on work performed in "HighEFF RA2.3 - Natural working fluids" and in "COPRO WP1 Enabling technologies" The in-house library for physical properties THERMPHYS has been used to evaluate exixting and investigate new models. Routines from THERMPHYS are used in both heat exchanger and in process simulation tools that are developed and used both in COPRO and HighEFF.

A number of viscosity models have earlier been implemented in the transport-property code THERMPHYS. These models where implemented mainly with CO_2 and CO_2 dominated mixtures in mind. Both COPRO and HighEFF investigates the design and operation of heat exchangers which uses hydrocarbon mixtures as the working fluid. In this work it is necessary to determine the transport properties of the working fluid over a wide temperature range, 250–400 K, and high pressures, 0.1–30 MPa. In this subtask we investigate the applicability of the models in THERMPHYS on various hydrocarbon mixtures, and we also discuss the possibility of implementing other viscosity models.

The thermal-conductivity models in THERMPHYS is sufficiently accurate for both single component and mixtures as long as the fluid is far away from the critical point. Close to the critical point the thermal conductivity is enhanced, but this enhancement is not included in THERMPHYS. The processes investigated in both COPRO and HighEFF often comes close to the critical point. We therefore investigate the thermal-conductivity model accuracy in this region, and the look into the possiblity for improvements.

2 Models for viscosity

There are many viscosity models available in the literature. They range from fully predictive theoretical models, to empirical correlations. Here we first present some correlations found in the literature, before we present two more sophisticated models based on the corresponding state principle.

2.1 Correlations

Correlations are enticing because of their relatively simple form and low computational cost. Typically, the empirical correlations can be accurate within some small range of parameters, but when used outside the domain determined by the experimental data they usually produce results with insufficient accuracy.

In a paper by Sanjari *et al.* [1] 4 such correlations where presented. These correlations are limited to natural gas with some impurities. The authors also present a new correlation based on 11 earlier experiments, with 4089 data points. The correlation is a rather simple function, $\eta = \eta(T_\mathrm{r}, P_\mathrm{r})$, where η is the viscosity, T_r (P_r) is the temperature (pressure) divided by the pseudo critical temperature (pressure) of the mixture. The exact form of $\eta(T_\mathrm{r}, P_\mathrm{r})$ can be found in the paper. In addition to this correlation we also investigated a correlation by Heidaryan *et al.* [2]. In this paper a correlation for the range of 320 - 400K and 3-140MPa was presented. A comparison with data calculated using Refprop [3] is shown in Fig. 1. Refprop is thought to give reasonable results, and is therefore used as a benchmark. The data produced by Heidaryan's correlation are very different from the data produced by Refprop. In Heidaryan's paper there are also experimental data, which was used to make this correlation. This data also fails to reproduce results of earlier experiments [4]. There is thus a mismatch to both the data from Refprop and data from earlier experiments. The correlation by Sanjari *et. al* on the other hand fits the Refprop data quite nicely, even for temperatures slightly outside the range of validity. Even so, the applicability of these correlations, and other correlations is very limited. For the purpose of robust process engineering

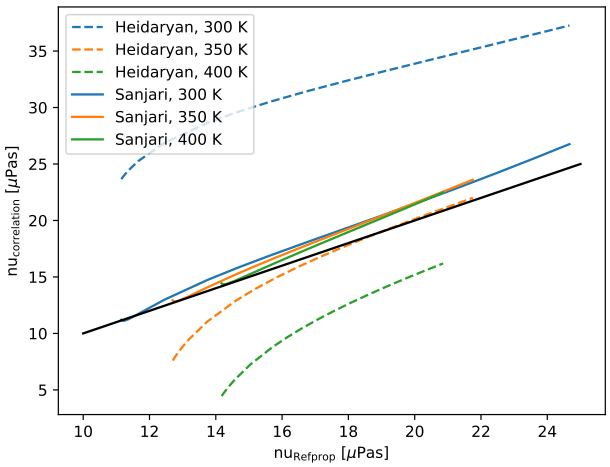

Figure 1: Comparison of viscosites produced by correlations with viscosites produced by Refprop. The data corresponds to pressures in the range 0.1-30 MPa. Black line: ideal data (guide to the eye).

calculations the viscosity model needs to be valid for more than (almost) pure fluids. With this in mind, it seems practically hopeless to manufacture a correlation which is sufficiently general.

2.2 The TRAPP method

In our in-house Fortran code, THERMPHYS, a corresponding state method for viscosity is implemented. This model, known as the TRAPP Method [5–7], uses a reference fluid for which the viscosity can be estimated accurately. In the form that it is implemented in THERMPHYS it uses propane as the reference fluid. Propane is chosen for two reasons, first of all an accurate correlation for the viscosity of propane exists, and secondly the freezing point of propane is very low relative to the critical temperature ($T_{\text{melt}} = 0.2T_{\text{crit}}$ at 1atm), which means it can be used over a wide range of temperatures. The model is semi-predictive, since only experimental data on the reference fluid must be known. We show the results of the model against experimental a relevant hydrocarbon mixture. in Fig. 2. The mixture is a binary mixture of pentane and octane. Here the Equation of State (EoS) PC-SAFT was used for the underlying density calculations for THERMPHYS. It should be noted that simpler EoSs such as Peng-Robinson and the Soave-Redlich-Kwong EoS produced much worse results in this particular case. We discuss the dependency of the the underlying EoS in more detail in the Result section, Sec. 3, below.

2.3 The two reference fluid model

The two reference fluid model (CS2), first presented in 1991 by Aasberg-Peteresen *et. al* [9], is a model based on the principle of corresponding states. As the name suggests, the model relies on two reference fluids instead of one. The rationale for using two reference fluids is to make a model that accounts for both light and heavy components by choosing a light reference fluid (LRF) and a heavy reference fluid (RFH). The viscosity of a mixture can be calculated from the viscosities of the reference fluids at the corresponding temperature and pressure (see Eq. (2)) and the critical viscosities of both the reference fluid and the mixture. The critical viscosities are calculated from

$$\eta_c = C \cdot m_{\text{w}}^{1/2} P_c^{2/3} T_c^{-1/6}, \tag{1}$$

where C is some unknown constant, m_{w} is the molar weight of the reference fluid or the mixture and P_c (T_c) is the critical pressure (temperature). The so called corresponding temperature and

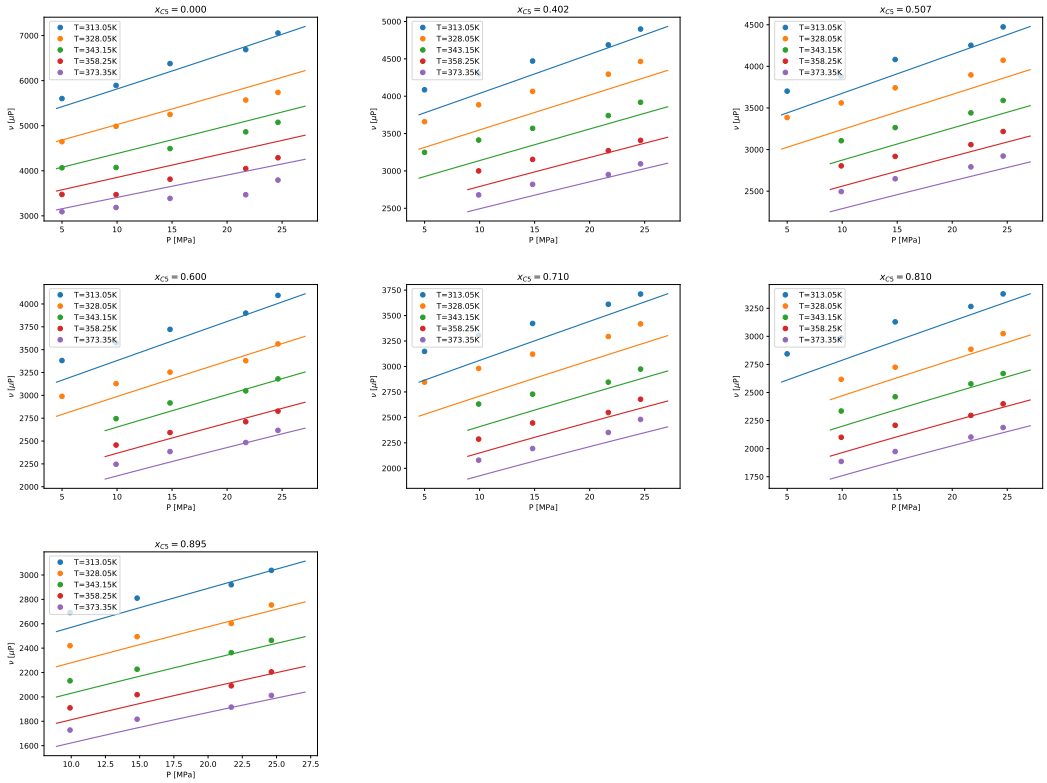

Figure 2: Comparison of results from THERMPHYS using PC-SAFT for density calculations on n-pentane – n-octane mixtures ($z = x_{C5}, 1 - x_{C5}$), and experimental results taken from Ref. [8].

pressure for reference fluid i are

$$T_i = T \frac{T_{c,i}}{T_{c,\text{mix}}}, \tag{2a}$$

$$P_i = P \frac{P_{c,i}}{P_{c,\text{mix}}}, \tag{2b}$$

where the subscripts $\{c, i\}$ and $\{c, \text{mix}\}$ denotes the critical properties of the reference fluid and mixture, respectively. The mixture viscosity can then be calculated from

$$\eta(T, P) = \eta_{c,\text{mix}} \frac{\eta_L(T_L, P_L)}{\eta_{c,L}} \left[\frac{\eta_H(T_H, P_H)}{\eta_{c,H}} \frac{\eta_{c,L}}{\eta_L(T_L, P_L)} \right]^K. \tag{3}$$

Here

$$K = \frac{m_{\text{w,mix}} - m_{\text{w},L}}{m_{\text{w},H} - m_{\text{w},L}}, \tag{4}$$

is the weight function which determines the relative dependency on RFL and RFH. For mixtures of low molecular weight close to that of RFL, $K \sim 0$, and η is dominated by the RFL properties. In the opposite case, for a heavy mixture with molecular weight close to that of RFH we get $K \sim 1$, and η is determined by the RFH properties. Here "mixture molecular weight" denotes a function that depends on the mole fractions, z_i, and molar weight of the mixture constituents, $m_{\text{w},i}$. Because large molecules contribute more to the the mixture viscosity than lighter molecules, Pedersen *et. al* [10] used the following expression for the mixture molecular weight

$$m_{\text{w,mix}} = m_{\text{w},n} + 0.00867358 \left(m_{\text{w},w}^{1.56079} - m_{\text{w},n}^{1.56079} \right), \tag{5}$$

where

$$m_{\mathrm{w},w} = \frac{\sum_{i=1}^{N} z_i m_{\mathrm{w},i}^2}{\sum_{i=1}^{N} z_i m_{\mathrm{w},i}}, \tag{6}$$

and

$$m_{\mathrm{w},n} = \sum_{i=1}^{N} z_i m_{\mathrm{w},i}. \tag{7}$$

The mixture critical temperature and pressure can be calculated from [11]

$$T_{c,\mathrm{mix}} = \frac{\sum_{i=1}^{N}\sum_{j=1}^{N} f_{ij}}{\sum_{i=1}^{N}\sum_{j=1}^{N} g_{ij}}, \tag{8a}$$

$$P_{c,\mathrm{mix}} = \frac{8\sum_{i=1}^{N}\sum_{j=1}^{N} f_{ij}}{\left[\sum_{i=1}^{N}\sum_{j=1}^{N} g_{ij}\right]^2}, \tag{8b}$$

where

$$f_{ij} = z_i z_j \left[(T_{c,i}/P_{c,i})^{1/3} + (T_{c,j}/P_{c,j})^{1/3}\right]^3 \left[T_{c,i}T_{c,j}\right]^{1/2}, \tag{9a}$$

$$g_{ij} = z_i z_j \left[(T_{c,i}/P_{c,i})^{1/3} + (T_{c,j}/P_{c,j})^{1/3}\right]^3. \tag{9b}$$

In the original paper Aasberg-Peteresen *et. al* used methane as the light component, and octane as the heavy component. The reasoning for using these components was that they were the lightest and heaviest hydrocarbon for which the viscosity was accurately known over a large range of T and P. Here we use methane and n-hexane as reference fluids, based on modifications made by Zeberg-Mikkelsen [12]. The reference fluid viscosities are then given by

$$\eta_i(\rho, T) = \eta_0(T) + \rho\eta_1(T) + \eta(\rho, T). \tag{10}$$

The viscosity is thus a sum of the dilute gas viscosity η_0, the first density correlation, η_1 and the η_2 which is the correlation term for high densities. The dilute gas viscosity is calculated from Chung's model [13], while η_1 and η_2 is calculated from the correlations

$$\eta_1(T) = A + B\left[C - \log\left(T/F\right)\right]^2, \tag{11a}$$

$$\eta_2(T, \rho) = H_2(T, \rho)\exp\left(j_1 + \frac{j_4}{T}\right), \tag{11b}$$

where

$$H_2(T, \rho) = -1 + \exp\left[\rho^{0.1}\left(j_2 + \frac{j_3}{T^{3/2}}\right) + \theta\rho^{0.5}\left(j_5 + \frac{j_6}{T} + \frac{j_7}{T^2}\right)\right], \tag{12}$$

and

$$\theta = \frac{\rho - \rho_c}{\rho_c}. \tag{13}$$

The coefficients, A, B, C, F, j_i, are listed in Table 1.

3 Results

The TRAPP method has density and temperature as inputs. Because of this, one must calculate the mixture density from T and P unless it is already known. This requires us to specify an EoS. Cubic EoS' are known for being easy to implement, and computationally cheap, however they are known to give inaccurate density calculations. Better density calculations can be expected if a more sophisticated EoS is used, such as PC-SAFT, or a multi-parameter EoS such as GERG2008. In Table 2 we compare results of TRAPP with density calculations for different EoS'. The cubic EoS'

Table 1: Coefficients for reference fluids

Coefficient	Methane	n-Hexane
A	5.117292274	-3927.003214
B	205.4216898	44.14835846
C	3.272931486	7.574428927
F	23.78006132	2387.565163
j_1	-9.964775064	-8.763923332
j_2	17.72167106	16.21397400
j_3	-2177.051453	-30767.16154
j_4	-92.52944093	1222.025332
j_5	-0.055509863	-0.020954437
j_6	256.5569447	232.0455992
j_7	5696.470962	101090.9658

Peng-Robinson (PR) and Soave-Redlich-Kwong (SRK) give inconsistent result, ranging from decent to terrible accuracy. Lee-Kesler is known for giving accurate density calculations and yield a more consistent accuracy. PC-SAFT give slightly better results, and so does GERG2008. Unfortunately, we where not able to calculate the density of hydrocarbons heavier than n-hexane using GERG2008.

Table 2: Average absolute relative error for THERMPHYS calculations for different mixtures (TRAPP unless CS2 is noted). a: Ref. [8], b: Ref. [14], c: Ref. [15]

Mixture	EoS	AARD (%)
nC5-nC8[a]	PC-SAFT	4.4
"	SRK	43
"	PR	9.0
"	LK	4.4
C1-nC4[b]	GERG2008	5.7
"	PC-SAFT	4.9
"	SRK	10
"	PR	18
"	LK	8.3
"	GERG2008 + CS2	5.9
C1-C2[c]	GERG2008	5.9
"	PC-SAFT	6.5
"	SRK	3.7
"	PR	20
"	LK	6.7
"	GERG2008 + CS2	6.8

Let us now compare results from TRAPP and CS2 with experimental results for some hydrocarbon mixtures. We use the GERG2008 EoS for density calculations. Additionally, we include results from Refprop. Fig. 3 shows data from an methane – ethane experiment. The TRAPP model overpredicts the viscosity at all temperatures and pressures, while the CS2 model underpredicts the viscosity. Both of these models show the correct functional form. The Refprop results are incredibly accurate.

In addition to the regular THERMPHYS calculations we include calculations from the CS2 model presented in the next sub-section. While for the n-pentane – n-octane mixture, the error seemed unsystematic, we here have a general overprediction made by THERMPHYS which increases as the temperature is lowered. Results on a methane-buthane mixture, shown in Fig. 4, have a similar

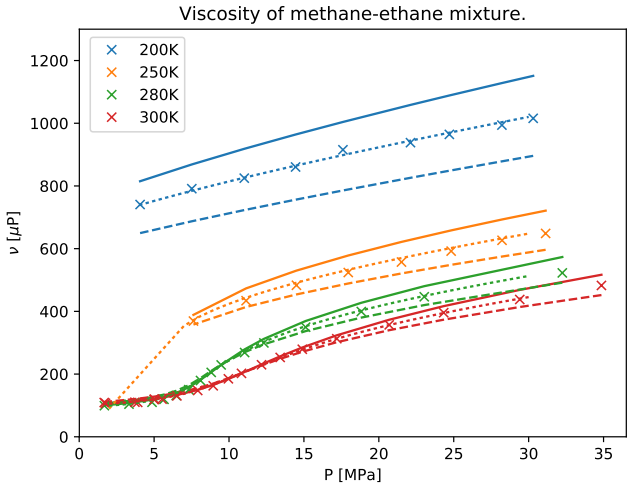

Figure 3: Comparison of calculated viscosities as a function of pressure with experimental data (×) at different temperatures for for a methane (50.2%) – ethane (49.8%) mixture. TRAPP (—) and CS2 (---) with GERG2008 and RefProp (···). The experimental results are taken from Ref. [15].

behavior. Also here Refprop produces the best over-all results, but at high temperatures results from CS2 are slightly better.

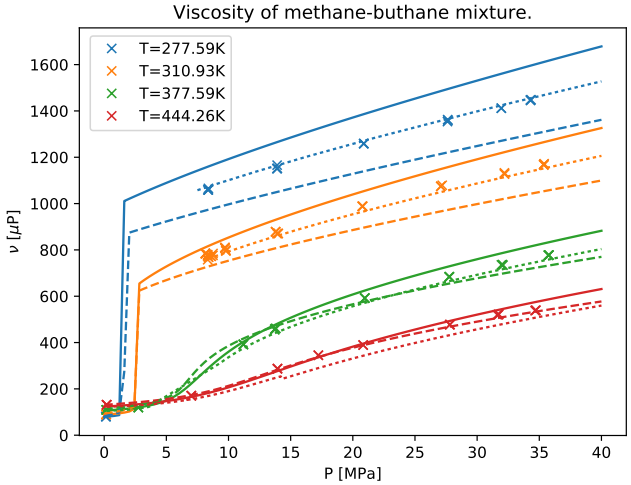

Figure 4: Comparison of calculated viscosities as a function of pressure with experimental data (×) at different temperatures for for a methane (39.4%) – buthane (60.6%) mixture. TRAPP (—) and CS2 (---) with GERG2008 and RefProp (···). The experimental results are taken from Ref. [14].

It is also interesting to see how well these models predict viscosities of hydrocarbons mixed with other fluids. In Fig. 5 we show results from a CO_2 – ethane mixture. Here the results of the CS2 model are more accurate up to $T = 260K$, and Refprop is more accurate at higher temperatures.

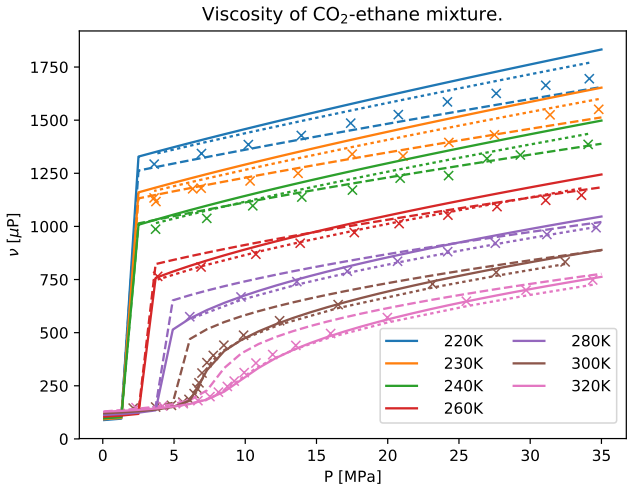

Figure 5: Comparison of calculated viscosities as a function of pressure with experimental data (×) at different temperatures for for a CO_2 (49.245%) – ethane (50.755%) mixture. TRAPP (—) and CS2 (---) with GERG2008 and RefProp (···). The experimental results are taken from Ref. [16].

4 Thermal conductivity

In this section we briefly present the present the models for high-pressure thermal conductivity. There is also a report on this from the project IMPACTS [17].

4.1 Current models

Prior to writing this document, there were two high-pressure thermal conductivity models implemented in THERMPHYS. Chung's model is described in detail by Poling *et al.* [7]. It uses the heat capacity and critical parameters of the mixture. It is not a corresponding-state method, so it does not need any measured conductivities. The model contains a parameter, ϵ, that is usually set to 1, that can be tuned to increase the accuracy for a specific mixture. The second model that has been implemented, is the TRAPP method for thermal conductivity. It is based on the same corresponding state principles as the TRAPP method for viscosity. In the standard implementation it uses propane as a reference fluid.

4.2 Extended corresponding states model

In Ref. [18] McLinden *et. al* presents a model for the thermal conductivity of refrigerants based on the extended corresponding state concept. This is the same concept that the TRAPP model is based on. The advatage with the implementation by McLinden *et. al* is that the model acounts for the enhancement of the thermal conductivity observed close to the critical point. The reference fluid is R134a. R134a is well studied, and accurate experimental data are readily available.

4.3 Model description

The model, like most thermal conductivity models, take the density, ρ, and temperature, T, as inputs. The thermal conductivity is split into three contributions,

$$\lambda(T,\rho) = \lambda_{\text{d.g.}}(T) + \lambda_r(T,\rho) + \lambda_{\text{crit}}(T,\rho). \tag{14}$$

Here, $\lambda_{\text{d.g.}}$ is the dilute contribution, so that $\lim_{\rho\to 0} = \lambda_{\text{d.g.}}$. The residual part, λ_r, accounts for the density contribution away from the critical point. λ_{crit} is the critical enhancement term. Far from

the critical point $\lambda_{\text{crit}} \ll \lambda_{\text{d.g.}}$. For a 1-component fluid the critical enhancement is theoretically infinite. Also for a mixture there is a strong enhancement, but it should not diverge at the critical point [18, 19].

Dilute thermal conductivity Because good models for the dilute thermal conductivity is already implemented in THERMPHYS, we will not present the model here. For single component thermal conductivity it is most accurate to simply do a polynomial fit to experimental data. These single-component values for the thermal conductivities are also used to calculate the mixture thermal conductivities. When no such polynomial is available, THERMPHYS has a fall back using Eucken's correlation for polyatomic gases [20]. To increase the accuracy of thermal-conductivity calculations for hydrocarbon mixture we are in the process of adding temperature polynomials for C_2 to C_6.

Residual part of the thermal conductivity The residual part of the thermal conductivity, λ_r, is found by first calculating the residual part of the reference fluid's thermal conductivity, λ_r^0, at the corresponding density and temperature. Let us first discuss the single component case. The mapping of temperature and density, $T, \rho \to T_0, \rho_0$, from the "real" T and ρ to the corresponding state point T_0, ρ_0 is done by mapping one equation of state onto another. If α_r is the reduced residual Helmholtz energy of the fluid, and α_r^0 is the reference fluids reduced residual Helmholtz energy, T_0, ρ_0 satisfies the equations

$$\alpha^r(T, \rho) = \alpha_0^r(T_0, \rho_0), \tag{15a}$$
$$Z(T, \rho) = Z_0(T_0, \rho_0), \tag{15b}$$

where Z is the compressibility factor. The solution can be represented in the form of shape factors, f and h:

$$T_0 = \frac{T}{f}, \tag{16a}$$
$$\rho_0 = \rho h. \tag{16b}$$

For a multi-parameter EoS it is difficult make a sufficiently robust solver for the equation set. We therefore simplify McLinden's model by using the same approach as in the TRAPP method for finding the shape factors. Once the shape factors are found the single-component thermal conductivity is found by evaluating

$$\lambda_r(T, \rho) = \lambda_r^0(T_0, \rho_0) F_\lambda, \tag{17}$$

where

$$F_\lambda = f^{1/2} h^{-2/3} \left(\frac{\text{mw}_0}{\text{mw}}\right)^{1/2}. \tag{18}$$

Here mw and mw_0 is the molar weight of the fluid and reference fluid, respectively. The residual thermal conductivity of the reference fluid, λ_r^0, is calculated with the formulation of Perkins *et al* [21]. Because Ref. [21] is not readily available, McLinden *et. al* includes the correlation in the articles appendix. Unfortunately, the equations are riddled with mistakes. We therefore include the formulation in Appendix A (hopefully with less mistakes). The formulation also requires access to accurate thermodynamical data for R134a. To this end, we have implemented the multi-parameter equation of state by Tillner-Roth and Baehr [22]. We have verified the accuracy of our implementation by comparison to experimental data on R134a.

The critical enhancement is treated similarly. The shape factors are not necessarily equal to 1 at the critical point. This requires some modification to ensure that the enhancement is centred at

the critical point. A simple adjustment, with no theoretical basis is made. Instead of evaluating the reference fluid's critical enhancement term at T_0, ρ_0, it is evaluated at

$$T_0^{\text{crit}} = T\frac{T_c^0}{T_c}, \tag{19}$$

$$\rho_0^{\text{crit}} = \rho\frac{\rho_c^0}{\rho_c}. \tag{20}$$

where the subscript c indicates the critical temperature, or density. Thus, $(T_0^{\text{crit}}, \rho_0^{\text{crit}}) = (T_c^0, \rho_c^0)$ at the critical point.

It turns out that this implementation, with the simplified shape factors, does not produce very accurate values for the thermal conductivity. There are two possible culprits. It is possible that the approximate shape factors differ to a too large extent from the "exact shape factors". A second option is that ρ_0 should be corrected by a thermal-conductivity shape factor: $\rho_0 = \chi h \rho$. This is has been done by Klein *et. al* [23], and McLinden *et. al* shows that using a simple density polynomial for χ reduces the average absolute deviation from 3% to 1.3% for R125. Since hydrocarbons are even more different from R134a, the improvement can possibly be even bigger. Unfortunately, we do not have the necessary coefficients available for testing a χ polynomial on a hydrocarbon.

Fortunately, there is a remedy to this problem. The TRAPP method also includes an additional correction factor, that is multiplied with the thermal conductivity,

$$\lambda^{\text{TRAPP}}(T, \rho) = \lambda_{\text{d.g.}}(T) + X_\lambda F_\lambda \lambda_r^0(T_0, \rho_0). \tag{21}$$

It is not clear (to me) what the theoretical basis for this correction factor is, but it might have something to do with inadequate shape factors. For a single-component fluid it takes the form

$$X_\lambda = \left[1 + \frac{2.1866(\omega - \omega_0)}{1 - 0.505(\omega - \omega_0)}\right]^{1/2}, \tag{22}$$

where ω (ω_0) is the acentric factor of the (reference) fluid. In our case, with the critical-enhancement term we use

$$\lambda(T, \rho) = \lambda_{\text{d.g.}}(T) + X_\lambda F_\lambda \left[\lambda_r^0(T_0, \rho_0) + \lambda_{\text{crit}}^0(T_{\text{crit}}^0, \rho_{\text{crit}}^0)\right] \tag{23}$$

Using this correction factor improves the result significantly.

The exact shape factors for mixtures are not surprisingly even more difficult to calculate. We therefore continue using the shape factors as calculated by the TRAPP method. For the critical-enhancement term the method requires calculation of the mixture's critical point. We use the Li method to calculate the critical temperature [24], and the density is calculated as the mole-averaged critical density. Neither of these methods are very accurate.

It turns out that our implementation of McLinden's model gives reasonable results close to the critical point, making it much more accurate than the TRAPP method in this region. Far away from the critical point the TRAPP method is more accurate than our calculations with McLinden's model. To utilize the qualities of both models we make a linear interpolation. Outside the region defined by the ellipse $(\rho_r - 1)^2/r_\rho^2 + (T_r - 1)^2/r_T^2 = 1$ we use the TRAPP method, and inside we let

$$\lambda = \lambda^{\text{McLinden}} w + \lambda^{\text{TRAPP}}(1 - w), \tag{24}$$

where

$$w = \sqrt{1 - (\rho_r - 1)^2/r_\rho^2 + (T_r - 1)^2/r_T^2}. \tag{25}$$

and the axes are set to $r_\rho = 1$ and $r_T = 0.2$. We dub this interpolation of the two models the TRAPP-McLinden model.

5 Results – Thermal conductivity

5.1 Ethane and propane single-component data

We compare the results from the TRAPP-McLinden model with experimental data on ethane and propane [25, 26]. The results are shown in Figures 6 and 7. from Ref. [26]. The results are shown in Fig. 7

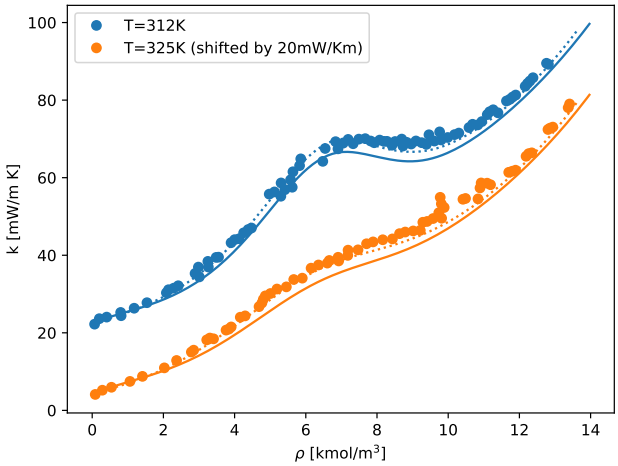

Figure 6: The thermal conductivity of ethane. Experimental data (o) from Ref. [25] compared to our TRAPP-McLinden model (—) and the RefProp model (---). The results for $T = 325$K was shifted down by 20 mW/Km to avoid overlap of the curves.

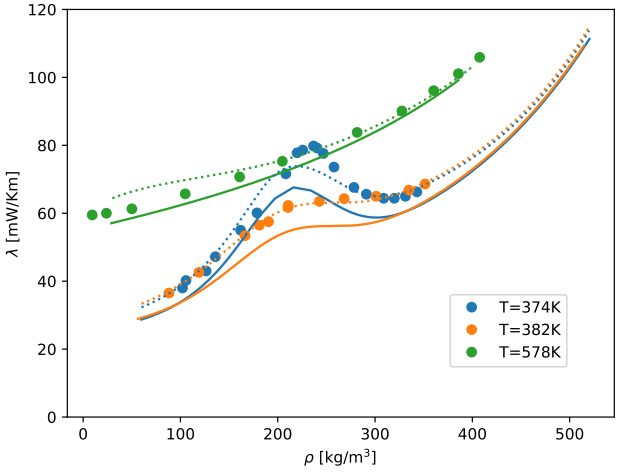

Figure 7: The thermal conductivity of propane. Experimental data (o) from Ref. [26] compared to our TRAPP-McLinden model (—) and the RefProp model (---).

5.2 Equimolar mixture of Methane and Ethane

We could obtain only one set of experimental data on a hydrocarbon mixture. Sakonidou *et. al* measured the thermal conductivity of a equimolar mixture of methane and ethane close to the critical point [19]. The results are shown in Fig. 8. We compare the results with calculations from

Refprop and the TRAPP-McLinden model. It is not clear why Refprop is so inaccurate for this mixture. The TRAPP-McLinden model has the correct shape, but the critical enhancement peaks at a temperature 3 K below the experimental data. This has a simple explanation. The method used to calculate the mixture's critical point is not very accurate, and underestimates the critical temperature with 3 K. We also show the results with a pre-calculated T_c

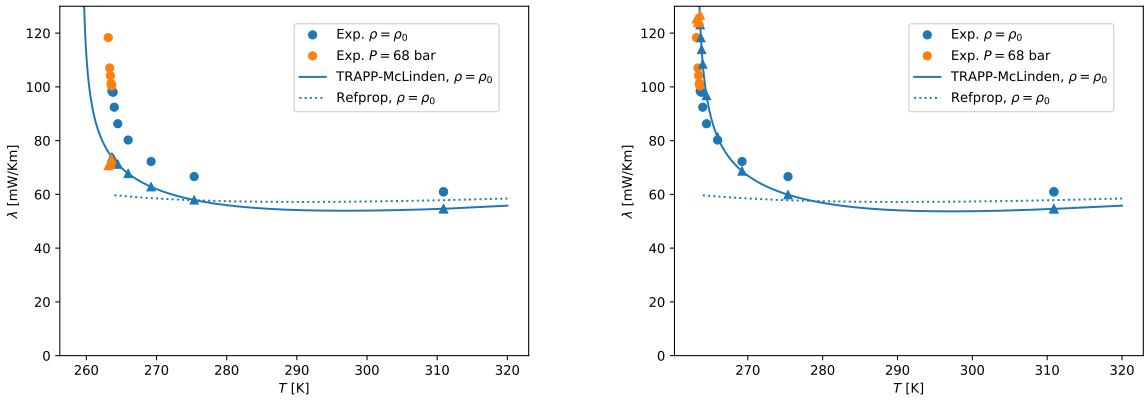

Figure 8: (Left) The thermal conductivity of a equimolar methane-ethane mixture. Experimental data (o) from Ref. [19] compared to our TRAPP-McLinden model (—) and the RefProp model (---). The experimental iso-lines are only approximately isochoric, or isobaric, and we therefore include the model results at the measured T and P (triangles). (Right) Same as left, with pre-calculated T_c and ρ_c. $\rho_0 = 8.5275\text{kmol/m}^3$.

It should be noted that Sakonidou *et. al* claims that $\rho_c = 8.5275\text{kmol/m}^3$, while we calculate $\rho_c = 8.8834\text{kmol/m}^3$ with GERG2008. This might explain why the state point calculations (triangles) are shifted along the curve relative to the experimental data (circles).

6 Conclusion

We have presented some of the available methods for calculating the viscosity of a hydrocarbon mixture at high pressures and temperatures. We conclude that it is practically impossible to make a sufficiently general correlation. The TRAPP method is quite accurate, but tends to overpredict the viscosity. The CS2 model has a similar accuracy, but underpredicts the results. It is important for both of these models that, when necessary, the density calculations are as accurate as possible. The results produced from Refprop are generally better than both these models, except for some mixtures at particular state points. One advantage of the CS2 model is that no density calculations are required.

The interpolation of the simplified McLinden model and the TRAPP model is a great improvement to only using the TRAPP model for calculating the thermal conductivity. Still, Refprop is a bit better for single-component fluids. For mixtures the available experimental data indicates that the TRAPP-McLinden model is accurate when the critical point of the mixture is pre-calculated. Since the experimental data is so sparse, we can not conclude with certainty that the apparent model accuracy is not accidental.

References

[1] E. Sanjari, E. N. Lay, and M. Peymani. “An accurate empirical correlation for predicting natural gas viscosity”. In: *Journal of natural gas chemistry* 20.6 (2011), pp. 654–658 (cit. on p. 2).

[2] E. Heidaryan, J. Moghadasi, and M. Rahimi. “New correlations to predict natural gas viscosity and compressibility factor”. In: *Journal of Petroleum Science and Engineering* 73.1 (2010), pp. 67–72 (cit. on p. 2).

[3] E. Lemmon, M. Huber, and M. McLinden. “REFPROP: Reference fluid thermodynamic and transport properties”. In: *NIST standard reference database* 23.8.0 (2007) (cit. on p. 2).

[4] I. K. Stephan and I. K. Lucas. “Empirical Estimation and Correlation Techniques”. In: *Viscosity of Dense Fluids*. Springer, 1979, pp. 15–17 (cit. on p. 2).

[5] J. F. Ely and H. Hanley. “Prediction of transport properties. 1. Viscosity of fluids and mixtures”. In: *Industrial & Engineering Chemistry Fundamentals* 20.4 (1981), pp. 323–332 (cit. on p. 3).

[6] J. Millat, J. Dymond, C. N. de Castro, and W. Wakeham. *Transport properties of fluids*. Cambridge University Press Cambridge, 1996 (cit. on p. 3).

[7] B. E. Poling, J. M. Prausnitz, J. P. O’connell, *et al. The properties of gases and liquids*. Vol. 5. Mcgraw-hill New York, 2001 (cit. on pp. 3, 8).

[8] M. A. Barrufet, K. R. Hall, A. Estrada-Baltazar, and G. A. Iglesias-Silva. “Liquid viscosity of octane and pentane+ octane mixtures from 298.15 K to 373.15 K up to 25 MPa”. In: *Journal of Chemical & Engineering Data* 44.6 (1999), pp. 1310–1314 (cit. on pp. 4, 6).

[9] K. Aasberg-Petersen, K. Knudsen, and A. Fredenslund. “Prediction of viscosities of hydrocarbon mixtures”. In: *Fluid phase equilibria* 70.2-3 (1991), pp. 293–308 (cit. on p. 3).

[10] K. S. Pedersen and A. Fredenslund. “An improved corresponding states model for the prediction of oil and gas viscosities and thermal conductivities”. In: *Chemical Engineering Science* 42.1 (1987), pp. 182–186 (cit. on p. 4).

[11] T. Leland, J. Rowlinson, and G. Sather. “Statistical thermodynamics of mixtures of molecules of different sizes”. In: *Transactions of the Faraday Society* 64 (1968), pp. 1447–1460 (cit. on p. 5).

[12] C. K. Zéberg-Mikkelsen. “Viscosity Study of Hydrocarbon Fluids at Reservoir Conditions: Modeling and Measurements”. PhD thesis. Ph. D. Thesis, 2001 (cit. on p. 5).

[13] T. H. Chung, M. Ajlan, L. L. Lee, and K. E. Starling. “Generalized multiparameter correlation for nonpolar and polar fluid transport properties”. In: *Industrial & engineering chemistry research* 27.4 (1988), pp. 671–679 (cit. on p. 5).

[14] L. Carmichael, V. M. Berry, and B. H. Sage. “Viscosity of a mixture of methane and butane”. In: *Journal of Chemical and Engineering Data* 12.1 (1967), pp. 44–47 (cit. on pp. 6, 7).

[15] D. E. Diller. “Measurements of the viscosity of compressed gaseous and liquid methane+ ethane mixtures”. In: *Journal of Chemical and Engineering Data* 29.2 (1984), pp. 215–221 (cit. on pp. 6, 7).

[16] D. E. Diller, L. J. Van Poolen, and F. V. Dos Santos. “Measurements of the viscosities of compressed fluid and liquid carbon dioxide+ ethane mixtures”. In: *Journal of Chemical and Engineering Data* 33.4 (1988), pp. 460–464 (cit. on p. 8).

[17] A. Austegard, J. Stang, and G. Skaugen. *Investigation of models for prediction of transport properties for CO2 mixtures*. Tech. rep. SINTEF Energy Research - Department of Gas Technology, 2013 (cit. on p. 8).

[18] M. O. McLinden, S. A. Klein, and R. A. Perkins. “An extended corresponding states model for the thermal conductivity of refrigerants and refrigerant mixtures”. In: *International Journal of Refrigeration* 23.1 (2000), pp. 43–63 (cit. on pp. 8, 9).

[19] E. Sakonidou, H. Van den Berg, C. Ten Seldam, and J. Sengers. “The thermal conductivity of an equimolar methane–ethane mixture in the critical region”. In: *The Journal of chemical physics* 109.2 (1998), pp. 717–736 (cit. on pp. 9, 11, 12).

[20] J. O. Hirschfelder, C. F. Curtiss, R. B. Bird, and M. G. Mayer. *Molecular theory of gases and liquids*. Vol. 26. Wiley New York, 1954 (cit. on p. 9).

[21] R. Perkins, A. Laesecke, J. Howley, M. Huber, and C. Nieto de Castro. “Experimental thermal conductivity and thermal diffusivity values for R32, R125, and R134a”. In: *National Institute of Standards and Technology, NISTIR (in preparation)* (1998) (cit. on p. 9).

[22] R. Tillner-Roth and H. D. Baehr. “An international standard formulation for the thermodynamic properties of 1, 1, 1, 2-Tetrafluoroethane (HFC-134a) for temperatures from 170 K to 455 K and pressures up to 70 MPa”. In: *Journal of Physical and Chemical Reference Data* 23.5 (1994), pp. 657–729 (cit. on pp. 9, 14).

[23] S. A. Klein, M. O. McLinden, and A. Laesecke. “An improved extended corresponding states method for estimation of viscosity of pure refrigerants and mixtures”. In: *International Journal of Refrigeration* 20.3 (1997), pp. 208–217 (cit. on pp. 10, 15).

[24] C. F. Spencer and R. P. Danner. “Prediction of bubble-point density of mixtures”. In: *Journal of Chemical and Engineering Data* 18.2 (1973), pp. 230–234 (cit. on p. 10).

[25] H. Roder and C. N. de Castro. “Thermal conductivity of ethane at temperatures between 110 and 325 K and pressures to 70 MPa”. In: *High Temperatures. High Pressures* 17.4 (1985), pp. 453–460 (cit. on p. 11).

[26] R. Tufeu and B. Le Neindre. “Thermal conductivity of propane in the temperature range 25–305 C and pressure range 1–70 MPa”. In: *International journal of thermophysics* 8.1 (1987), pp. 27–38 (cit. on p. 11).

A Thermal conductivity of R134a

This is a short description of the thermal conductivity correlation for R134a. The multi-parameter EoS by Tillner-Roth and Baehr [22] has been implemented in thermopack. This is used to find the pressure, $P(T,\rho)$ and calculate the pressure susceptibility of the density, $\left(\frac{\partial\rho}{\partial P}\right)_T$. The EoS has typical accuracies of less than 0.05% for the densities.

The correlation consists of the dilute-gas contribution, the residual part and the critical-enhancement term

$$\lambda(T,\rho) = \lambda_{\mathrm{d.g}}(T) + \lambda_{\mathrm{r}}(\rho) + \lambda_{\mathrm{crit}}(T,\rho). \tag{26}$$

Here we have dropped any sub/superscript 0 indicating that this is the reference fluid for brevity. All properties in this section are R134a properties.

Although it is not used in our calculations, we include the dilute-gas term for completeness. It is just a linear function in T,

$$\lambda_{\mathrm{d.g.}} = a_0 + a_1 T, \tag{27}$$

where $a_0 = -1.05248 \cdot 10^{-2}\mathrm{W/mK}$ and $a_1 = 8.0982 \cdot 10^{-5}\mathrm{W/mK^2}$.

The residual part is represented as a quartic polynomial in the reduced density, $\rho_r = \rho/\rho_c$:

$$\lambda_r = \lambda_{\mathrm{reducing}} \sum_{i=1}^{4} b_i \rho_r^i \tag{28}$$

Table 3: Coefficients for λ_r^0

Coefficient	Value
$\lambda_{\text{reducing}}$	$2.055 \cdot 10^{-3}$W/mK
b_1	1.836526
b_2	5.126143
b_3	-1.436883
b_4	0.626144

The coefficients are listed in Table 3.

The critical enhancement is

$$\lambda_{\text{crit}}(T,\rho) = \rho c_p \frac{R_0 k_B T}{6\pi\eta\xi}(\Omega - \Omega_0), \tag{29}$$

where c_p is the isobaric heat capacity, $R_0 = 1.03$ is a universal amplitude, k_B is Boltzmann's constant, $\eta = \eta(T,\rho)$ is the viscosity, ξ is a correlation length, and Ω and Ω_0 are crossover functions. Thus an accurate correlation for the viscosity is required. We use the recommended viscosity correlation by Klein *et. al* [23]. We do not present this correlation here as it is rather involved (contains about 55 coefficients) and the presentation by Klein *et. al* is quite straightforward.

The correlation length is given by

$$\xi(T,\rho) = \frac{\xi_0}{\Gamma}\left[\chi^*(T,\rho) - \chi^*(T_{\text{ref}},\rho)\frac{T_{\text{ref}}}{T}\right]^{\nu/\gamma}, \tag{30}$$

where χ^* is a dimensionless susceptibility,

$$\chi^*(T,\rho) = \frac{\rho P_c}{\rho_c^2}\left(\frac{\partial\rho}{\partial T}\right)_T. \tag{31}$$

$\xi_0 = 1.94 \cdot 10^{-10}$ m is the critical amplitude, $\Gamma = 0.0496$, T_{ref} is a reference temperature set to $T_{\text{ref}} = 1.5T_c$. The universal exponents are $\nu = 0.63$ and $\gamma = 1.239$. The crossover functions are

$$\Omega(T,\rho) = \frac{2}{\pi}\left[\frac{c_p - c_v}{c_p}\arctan(q_D\xi) + \frac{c_v}{c_p}q_D\xi\right] \tag{32}$$

and

$$\Omega_0(T,\rho) = \frac{2}{\pi}\left[1 - \exp\left(-\frac{1}{(q_D\xi)^{-1} + (q_D\xi\rho_c/\rho)^2/3}\right)\right]. \tag{33}$$

Here c_v is the isochoric heat capacity. The typical uncertainty of the thermal-conductivity correlation is 5%.